DOI:10.1021/jf103243m

JOURNAL OF AGRICULTURAL AND FOOD CHEMISTRY
ARTICLE

Homology Modeling and Screening of New 14α-Demethylase Inhibitor (DMI) Fungicides Based on Optimized Expression of CYP51 from *Ustilago maydis* in *Escherichia coli*

Rui Han,[∥,†,‡] Jianhua Zhang,[∥,†] Shuxiang Li,[†] Shufen Cao,[†] Hui Geng,[†] Yongze Yuan,[†] Wenjing Xiao,[§] Shenghua Liu,[§] and Deli Liu*[,†,§]

[†]Hubei Key Laboratory of Genetic Regulation and Integrative Biology, College of Life Science, Huazhong Normal University, Wuhan 430079, China, [‡]Institute of Horticulture, Qinghai Academy of Agriculture and Forestry, Qinghai University, Xining 810016, China, and [§]Key Laboratory of Pesticide and Chemical Biology (CCNU) of Ministry of Education, Wuhan 430079, China. [∥] These authors contributed equally.

Ustilago maydis infection is a serious disease affecting corn crops worldwide. Sterol 14α-demethylase (CYP51) is one of the key enzymes of sterol biosynthesis and an effective target of antifungal drugs. To further study the interaction between CYP51 and drugs and exploit more specific 14α-demethylase inhibitor (DMI) fungicides for *U. maydis*, in this study homology modeling of CYP51 from *U. maydis* (UmCYP51) templated as the eukaryotic orthologues (the human CYP51) and screening of new DMI fungicides based on optimized expression were carried out for the first time. In addition, XF-113 and ZST-4 were screened by analyzing the spectral characteristics between the purified UmCYP51-35 and fungicides. These results provide a theoretical basis and new ideas for efficient design and development of new antifungal drugs.

KEYWORDS: CYP51; *Ustilago maydis*; homology modeling; optimized expression; site-directed mutagenesis; DMI fungicides

INTRODUCTION

Corn smut, caused by *Ustilago maydis*, is one of the most serious diseases affecting cultivated corn. It has been reported that sterol 14α-demethylase ($P450_{14DM}$ or CYP51) is a critical enzyme for *U. maydis* survival (*1*). CYP51 is a member of the P450 family of proteins, which are widely distributed in prokaryotes and eukaryotes. It catalyzes the three-step reaction of sterol 14α-demethylation. In fungi, the complex sterol 14α-demethylation reaction presents one of the key steps in sterol biosynthesis, an essential metabolic pathway producing ergosterol (*2*). The depletion of ergosterol results in the accumulation of methylated sterol precursors, affecting both membrane integrity and the function of membrane-bound proteins and eventually causing inhibition of fungal growth. Inhibitors of fungal sterol 14α-demethylase, termed demethylase inhibitors (DMIs), are the main group of fungicides used in agriculture and medicine. Azoles are the most widely used and studied class of antifungal agents in both agricultural and medicinal usage; however, the broad usage of these compounds leads to the development of resistance. Therefore, the invention of new and effective antifungal agents is of great importance (*3*).

Because lanosterol 14α-demethylase (CYP51) is a prime target for the development of antifungal drugs (*4*), the study of CYP51 is becoming a research hotspot in agriculture (*5*), and the expression of CYP51 genes has been extensively investigated in *Magnaporthe grisea*, *Penicillium digitatum*, *Antrodia cinnamomea*, and *Penicillium italicum* (*6*−*9*). Until now, a few expression systems, for example, *Escherichia coli*, *Saccharomyces cerevisiae*, *Schizoasccharomyces pombe*, and *Pichia pastoris*, and insect cell and mammalian cell systems were used for expressing CYPs. Microsomal *M. grisea* CYP51 and *P. digitatum* CYP51 have been expressed successfully in *E. coli*. Although UmCYP51 has been previously expressed in yeast (*10*), there is no report on the expression in *E. coli*, which is widely used and has several advantages, including low cost, no endogenous single-oxidase system, and so on.

However, due to the membrane character of the fungus enzyme (CYP51), it was very difficult to express CYP51 soluble. Thus, molecular modeling of CYP51 structure has been used extensively to explain possible protein−drug interactions. This provides an insight into which residues in the protein seem to be important in the binding of the ligand and how the candidate could be modified to increase or decrease its affinity for a particular target (*11*, *12*). There are only a few reports on the crystal structure of P450-14DM (CYP51), including the crystal structure of *Mycobacterium tuberculosis* CYP51 and the human and *Trypanosoma brucei* CYP51 (*13*−*15*). Although some homology models such as CYP51 from *M. grisea* and *P. digitatum* were attained on the basis of the crystal structure of *M. tuberculosis* CYP51 (*5*,*6*), this may not be a suitable template for the analysis of eukaryotic orthologues. Compared with the other two, the human CYP51 is the second structure of a eukaryotic microsomal P450-14DM that acts on sterol biosynthesis, and it differs profoundly from that of the water-soluble CYP51 family member

*Corresponding author (phone 0862767865534; fax 0862767861936; e-mail deliliu2002@yahoo.com.cn).

 Published on Web 11/23/2010

from *M. tuberculosis*, both in organization of the active site cavity and in the location of substrate access channel.

In this study, homology modeling and screening of new DMI fungicides for UmCYP51 based on optimized expression were carried out for the first time. The three-dimensional (3D) model of UmCYP51 was created using the human CYP51 as template and was confirmed with high reliability by site-directed mutagenesis; two truncated mutants, UmCYP51-20 and UmCYP51-35, were constructed by subcloning the truncated genes into different vectors and expression in different host strains. Expression results revealed that only pET32-Um-35 could be highly expressed in *E. coli* BL21 (DE3). The purified recombinant UmCYP51-35 was used as the target enzyme to select a new inhibitor from the synthetic XF and ZST compounds for the first time. Our results indicate that only compounds XF-113 and ZST-4 had similar binding constants when compared with commercial fungicides. These structural characteristics regarding the interaction between heterogeneous UmCYP51 and fungicides analyzed by homology modeling, binding assay, and site-directed mutation will provide essential information for designing potent fungicides and guiding the control of pathogens in agriculture.

MATERIALS AND METHODS

U. maydis was obtained from the China General Microbiological Culture Collection Center. *E. coli* BL21 (DE3), BL21 (DE3) pLysS, and Rosetta (DE3) strains and plasmids pET-32, pET-28, and pGEX-KG were stored in our laboratory. Diniconazole, tebuconazole, triadimenol, and triadimefon were purchased from the Factory of Limin (Yancheng, China). XF and ZST series compounds were provided by Chemistry College of Central China Normal University. Ni-NTA affinity resin was purchased from Novagen (Germany).

Structural Analysis and Homology Modeling of the *U. maydis* CYP51. The secondary structure of UmCYP51 was predicted using online tools (http://www.expasy.ch/tools/) (*16*). All fungal CYP51 proteins were transmembrane proteins, and the entire protein sequence was analyzed (http://www.cbs.dtu.dk/services/TMHMM/) (*17*). The 3D model of the UmCYP51 (ID: P49602) was built on the basis of the template of human CYP51 (PDB, 3LD6) using the Modeler 9v4 program after sequence alignment using ClustalW (http://www2.ebi.ac.uk/CLUSTALW) with a gap penalty of 10 and BLOSUM series weight matrix. Modeler generates the 3D models by optimization of molecular probability density functions. The refinement of the model was achieved by scanning main-chain and side-chain torsions to relieve unacceptable van der Waals contacts. The backbone of the model was defined and held as an aggregate, whereas the remainder of the model was minimized by the Powell method (conjugate-gradient minimizer) using the Tripos Force Field (Tripos 7.0). Finally, the aggregate was removed and the protein minimized as a whole. To investigate further the binding of azole antifungal agents with the enzyme, tebuconazole was docked into the active site of the refined UmCYP51 structure using AutoDock version 4.0 (*18*). The AutoDock Tools kit was used to prepare the required structures for docking. Superposition of the model of UmCYP51 and the template human CYP51 was performed.

Cloning *U. maydis* CYP51 and Construction of Expression Vectors. The genomic DNA was extracted from *U. maydis* cultured in potato dextrose broth (PDB) at 25 °C for 3 days and was used as a template for amplifying the CYP51 gene. The primers were designed on the basis of published sequence data (DDBJ ID: Z48164). The forward primer Pf containing a *Kpn*I recognition site (underlined) was 5′-GGGGTACCATGGTGGCCTCC TCGTCTTC-3′, and the reverse primer Pr was 5′-CGGAATTCCTAGTCGAGGTGGAGGGATTCG-3′ containing an *Eco*RI recognition site (underlined). The amplified fragments were cloned into the pMD18-T easy vector (TaKaRa Bio Inc., China). Construction of the recombinant plasmids to express the truncated forms of CYP51 required two sets of primers. For UmCYP51-20 (with 60 bp deletions in the 5′-terminal sequence of the UmCYP51 gene coding for 20 amino acids at the N-terminal), the primers sequences were Pf_{-20} 5′-CGAATTCATGC-TCGCCGATTCTTCGGC-3′ and Pr_{-20} 5′-CAAGCTTATTAGTCGAG GTGGAGGGATTC-3′, with each primer containing recognition sites (underlined) for *Eco*RI and *Hin*dIII, respectively. The primer sequences used for UmCYP51-35(with 105 bp deletions in the 5′-terminal sequence of the UmCYP51 gene coding for 35 amino acids at the N-terminal) were Pf_{-35} 5′-GGAATTCATGTTGCTTCCATTGCTCGCG-3′ and Pr_{-35} 5′-CAAGCTTATTAGTCGAGGTGGAGGGATTC-3′, with each primer containing the same recognition sites (*Eco*RI and *Hin*dIII, underlined). After digestion with the restriction enzymes mentioned above, all amplified fragments were inserted into pET-28, pET-32, or pGEX-KG successfully and analyzed by Blast (http://www.ncbi.nlm.nih.gov/BLAST/). The six His tags were incorporated into the N-terminal of the fusion protein to make the recombinant protein bind easily to the Ni-NTA column, which was capable of facilitating the purification procedure.

Table 1. Analysis of Binding Constants for the Mutant Proteins against Various Fungicides[a]

	K_d (μM)			
	protein	mutant protein		
fungicide	UmCYP51-35	Y95F	F206L	H293D
tebuconazole	0.110	0.704	0.408	no binding
diniconazole	0.255	0.914	0.765	no binding

[a] UmCYP51-35, with 60 bp deletions in the 5′-terminal sequence of the UmCYP51 gene coding for 35 amino acids at the N-terminal. Spectroscopic binding (K_d) assays were repeated three times.

Optimized Expression in *E. coli* and Purification of UmCYP51. All recombinant plasmids were transformed into *E. coli* BL21 (DE3) and selected with appropriate antibiotics. To obtain optimal protein expression, *E. coli* BL21 was induced using different IPTG concentrations (0.1, 0.5, and 1 mM) and different temperatures (37, 30, and 20 °C) for 6 h. The following host strains were also examined: BL21, pLysS (DE3), and Rosetta (DE3). After harvest by centrifugation, the cells were resuspended in precooled lysis buffer (100 mM NaH_2PO_4, 10 mM Tris-Cl, 10 mM imidazole, pH 8.8) and lysed by sonication on ice at an intensity of 120 W for six cycles of 60 s pulses, with a 10 s rest between bursts. The supernatant containing the six His-tagged proteins was purified using Ni-NTA affinity resin according to the manufacturer's protocol (Novagen). The purified protein was analyzed by SDS-PAGE, and protein concentration was determined according to the Bradford method using bovine serum albumin (BSA) as a protein standard (*19*). The activity and content of UmCYP51 were determined by using the Omura and Sato method (*20*).

Construction of Mutants and Analysis of Binding Capacity. The amino acid residues in the active site of the target enzyme can affect its interaction with drugs. Combined the amino acid residues (Tyr 95, Val 108, Phe116, Phe206, Ala 286, His293) in the cavity of active sites based on the 3D structural model of UmCYP51 with the homology comparison between UmCYP51 and six other filamentous fungi, the Tyr95, His293, and Phe206 sites were chosen for site-directed mutagenesis. Mutant primers for PCR amplification were designed according to the manufacturer's instructions in the Muta-direct site-directed mutation primer design kit (SBS Genetech Co., Ltd.). The recombinant plasmids were transformed into *E. coli* BL21. The activity and binding ability to fungicides of the mutant protein were detected by an S-3100 UV−vis spectrophotometer, and the binding constants were analyzed (**Table 1**).

Screening of New DMI Fungicides Targeted UmCYP51. A final concentration of 0.25 mg mL^{-1} recombinant protein (UmCYP51-35) was prepared, and the scanning baseline between 350 and 500 nm was determined. The absorption spectrum of a 2 min response was detected by an S-3100 UV−vis spectrophotometer (Scinco Co. Ltd.) after the addition of four standard fungicides at different concentrations (0.1−20 μM). Type II binding spectra were measured as described previously (*21*). The margins of peaks and troughs were analyzed according to absorption spectra, and the binding constants were calculated by using the Hanes−Woolf mapping method (*22*). The binding properties of the recombinant CYP51-35 protein with the synthetic XF and ZST fungicide compounds were determined in the same way.

RESULTS AND DISCUSSION

Transmembrane Prediction and Homology Modeling Analysis of *U. maydis* CYP51. It was reported that fungal CYP51s are

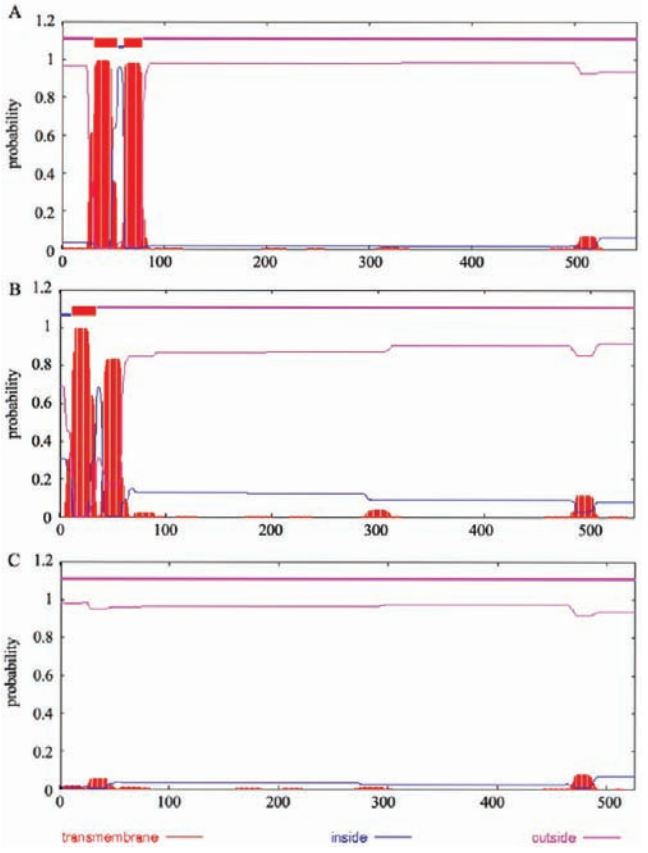

Figure 1. Transmembrane region analysis of *U. maydis* CYP51s: (**A**) the whole sequence of UmCYP51 using TMHMM 2.0; (**B**) truncated N-terminal 20 amino acids (UmCYP51-20); (**C**) truncated N-terminal 35 amino acids (UmCYP51-35).

membrane-bound proteins and that their transmembrane domains are located at the N-terminal (*17*). The N-terminal transmembrane domain may play a role in the regulation of positioning and expression and, to a lesser extent, its function, and may have an effect on its heterologous expression. Topology prediction (TMHMM) indicated that UmCYP51 had two transmembrane regions that were not necessary for normal UmCYP51 function (**Figure 1A**). Because the UmCYP51 gene was not expressed in *E. coli*, the 5′-terminal sequences (60 or 105 bp) encoding the corresponding amino acids in the N-terminal transmembrane region were truncated, and the transmembrane structures were predicted. The results demonstrated that there was one transmembrane domain in the UmCYP51 when 20 amino acids were truncated from the N-terminal (**Figure 1B**), whereas there was no transmembrane domain when 35 amino acids were removed (**Figure 1C**).

Because no 3D structure was available for UmCYP51, a molecular model to visualize the sites of labeling was created. As part of our research project, the 3D model of UmCYP51 was built on the basis of the structure template of human UmCYP51 using the Modeler 9v4 program (**Figure 2A**). There was 40% identity between sequences of UmCYP51 and human CYP51. Their topologies were quite similar, and most of the secondary and supersecondary structural motifs, characteristically hydrophobic and hydrophilic segments, and the regions of the sequence containing the heme binding site, the oxygen binding site, and the site of interactions with redox partners were highly conserved. The 3D structural model of UmCYP51 is overall similar to those of other CYPs reported previously and exhibits a closed conformational form with the active site deeply buried in the center of the structural fold. The heme group is sandwiched between helices I and L (the secondary structure nomenclature is referred to the template). The active site above heme is mainly composed of hydrophobic residues. Many available fungus CYP structures reveal that a highly conserved threonine is located in the middle of helix I. This conserved residue has been suggested to participate in the proton delivery and plays an important role in dioxygen bond cleavage during the catalytic cycle (*13*). **Figure 2B** shows the superposition of the UmCYP51 model with the human CYP51. As expected, the overall conformation of the model was very similar to the template, with a rmsd of 0.658. There were little differences between CYP51 and the mutants in the external structure, and the heme active sites appeared to be almost identical in the 3D models. With the effective docking of tebuconazole in the active site of both full-length and mutant CYP51 models, the results verified that the enzyme activity remained the same and indicated that residues Tyr95, Thr99, Val108, Phe116, Phe206, Ala 286, His293, and Thr298 constitute the cavity of the active site (**Figure 2C**).

The human CYP51 is the second structure of a eukaryotic microsomal CYP51 that acts on sterol biosynthesis, and it differs profoundly from that of the water-soluble CYP51 family member from *M. tuberculosis*, both in organization of the active site cavity and in the access channels for ligand binding (*14*). Structural differences between the human CYP51 and MtCYP51 explain both the low efficacy of MtCYP51-based homology modeling in predicting potencies for the inhibitors aimed to target 14DMs from eukaryotic pathogens and the limited applicability of the MtCYP51 structure in understanding structure−function relationships in the CYP51 family (*15*). The above allowed us to predict that the human CYP51 structure will serve as a good model for other eukaryotic CYP51 orthologues.

Optimized Expression in *E. coli* and Purification of UmCYP51. The *cyp*51 gene of *U. maydis*, Um*cyp*51-20, and Um*cyp*51-35 were cloned and validated by sequencing and then successfully inserted in different expression vectors with *Hin*dIII/*Sac*I digestion. These recombinant expression vectors were transformed into different hosts (BL21(DE3), BL21(DE3) pLysS, Rosetta-(DE3)), and unfortunately most of them were not expressed. After many attempts, only pET32-Um-35, encoding UmCYP51-35, could be highly expressed in *E. coli* BL21 (DE3) at 30 °C with 0.5 mM IPTG (**Figure 3**). The entire UmCYP51 protein and the other truncated UmCYP51-20 protein could not be expressed in the *E. coli* system. The reason may be the second transmembrane region playing a very important role in the expression.

The above result indicated that the truncation of N-terminal amino acids in UmCYP51 was critical for its successful expression in *E. coli*, which was consistent with prior studies on the prokaryotic expression of P450 and other membrane proteins. One example is cholesterol 7α-hydroxylase (CYP7A1), which was expressed in *E. coli* by modifying amino acids at the N-terminal end (*23*); its activity was not affected by cytochrome P450 reductase (CPR) when 33 amino acids at the N-terminus, encoding the transmembrane domains, were truncated (*24*). Recently, *T. bruceibrucei* (Tbb) P450-14DM was highly expressed in *E. coli* by replacing its N-terminal transmembrane domain upstream of P32 with the MAKKTSSKGKL N-terminal sequence from CYP2C3 (*15*).

Only BL21 (DE3), not BL21(DE3) pLysS, or Rosetta(DE3), is appropriate for expression, which indicated that rare codens have little influence in the expression of UmCYP51. The vectors pET-32 and pGEX-KG were chosen to express the full-length UmCYP51 according to fusion protein, but they could not be expressed successfully. Maybe the N signal peptide of UmCYP51 has certain inhibition of the expression or the secondary structure of RNA has changed significantly during the transcription and translation. Only pET32-Um-35 can be expressed, not other

Figure 2. Homology modeling of UmCYP51: (**A**) is a ribbon schematic representation of the homology model of UmCYP51. Heme is shown as a green stick. The image was generated using PyMOL (http://www.pymol.org). (**B**) The model of UmCYP51 (Carmine) was superimposed on the template: the human CYP51 (loden). (**C**) is the docking conformation of tebuconazole (light blue) in the active site of UmCYP51 model.

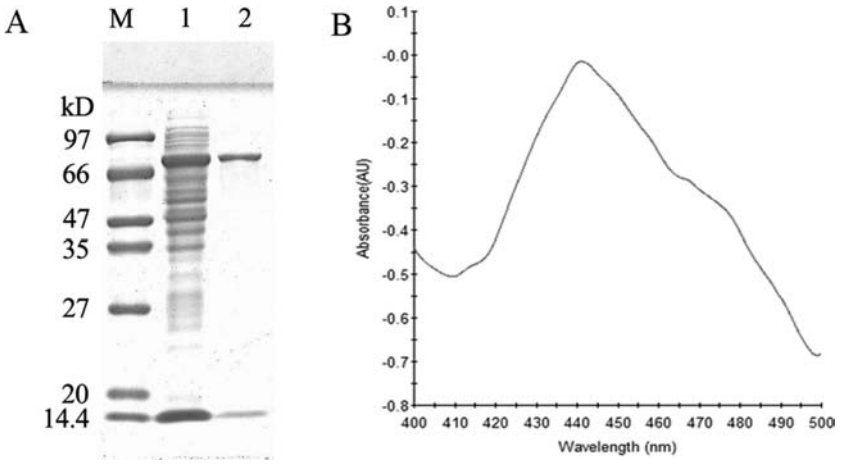

Figure 3. Purification and activity analysis of UmCYP51-35 expressed in *E. coli*: (**A**) expression and purification of UmCYP51-35 analyzed by SDS-PAGE (lanes: M, low molecular weight protein standard; 1, total protein expressed by *E. coli*; 2, purified protein obtained by Ni-NTA column chromatography); (**B**) differential CO-reduced spectrum of purified UmCYP51-35.

expression vectors, which showed it was associated with pET32, which contains a special fusion protein gene. The expression mechanism remains for further study.

Obtaining a sufficient quantity of CYP51 protein from *U. maydis* was a major hurdle in studying the interaction between the protein and fungicides. UmCYP51-35 was heterologously expressed in *E. coli* for the first time in this study. *E. coli* was the ideal expression system, lacking interference from cytochrome P450 as it is absent from *E. coli*. The recombinant UmCYP51-35 was largely expressed and purified using a Ni-NTA resin. SDS-PAGE indicated a single band with an approximate molecular mass of 70 kDa that was the UmCYP51-35 His-tagged fusion protein (**Figure 3A**).

The CYP51 Fe(II)−CO complex in the "active" form has a Soret band maximum close to 450 nm (P450), whereas the "inactive" form has a maximum absorbance near 420 nm (P420). The UmCYP51-35 expressed in *E. coli* revealed a typical absorbance spectrum of reduced CO spectrum with a maximum at 445 nm (**Figure 3B**). The concentration of UmCYP51-35 was 3.763 pmol mg^{-1} of total protein.

Site-Directed Mutagenesis of UmCYP51. The homology of UmCYP51 with six other filamentous fungi was low, at about 30% amino acid identity. However, the amino acid residues in the substrate recognition sites (SRSs) were highly conserved and concentrated in the SRS1 and SRS4 domains (**Figure 4**). Some of the amino acids in SRS1 and SRS4 may have a direct impact on drug interaction. The Tyr95 and His293 sites were highly conserved in all living organisms, whereas the Phe206 site was located in the F-helix zone and found to be conserved in fungi only. By combination of the amino acid residues in the active sites based on the 3D structural model of UmCYP51 with the homology comparison between UmCYP51 and six other filamentous fungi, Tyr95, Phe206, and His293 were chosen for site-directed mutagenesis, and three recombinant plasmids containing the Y95F, F206L, or H293D mutation were constructed. Following transformation into *E. coli* BL21, the mutant UmCYP51s were highly expressed and revealed a typical absorbance spectrum of reduced P450. The binding affinities of the three purified mutant UmCYP51s with tebuconazole and diniconazole were tested, and the results indicated that mutations in the Tyr95, Phe206, and His293 sites affected drug interaction. The binding of tebuconazole and diniconazole with the mutated UmCYP51s induced a typical type II spectrum with a peak at 430 nm and a trough at 400 nm. The K_d values of the mutant and wild-type proteins binding with fungicides are shown in **Table 1**. The K_d values of the Y95F and F206L mutants binding with fungicides were greater than those of the wild type, whereas the H293D mutant was not able to bind with the fungicides tested.

Tebuconazole had the best binding affinity with the wild-type protein; however, the increased K_d values with the Y95F and F206L mutants indicated that this affinity with tebuconazole was decreased with these particular mutants. These results showed that the Tyr95 and Phe206 sites played a role in UmCYP51 binding with tebuconazole and that Phe206 might be a target site of high-specificity UmCYP51 inhibitors. The H293D mutant lacked any binding ability to the fungicides tested, implying that the His293 site might be involved in maintaining the spatial structure of UmCYP51.

As the alteration of some critical amino acid residues within the active site of the target enzyme (CYP51) was assumed to alter the

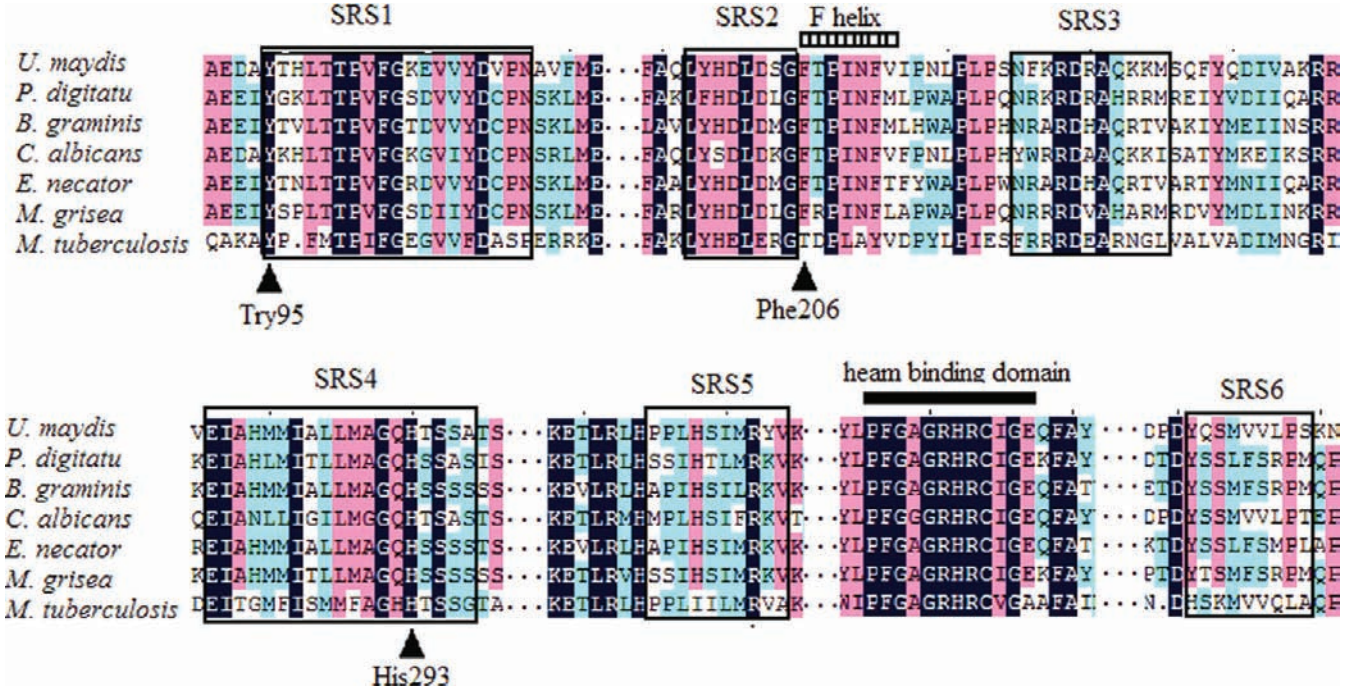

Figure 4. Multiple alignments of various fungi and UmCYP51 sequences. The key residues of UmCYP51 interacting with azoles are marked with the symbol ▲. Substrate recognition sites (SRSs) are indicated by the boxed regions. The F-helix and the heme binding domain are also clearly marked.

Table 2. Analysis of Binding Constants for Fungicidal Compounds against Recombinant UmCYP51-35[a]

fungicide	K_d (μM)	fungicide	K_d (μM)
		Standard	
tebuconazole	0.110	diniconazole	0.255
		Synthetic	
XF-22	0.679	XF-36	0.798
XF-38	1.647	XF-40	1.383
XF-49	1.160	XF-62	0.984
XF-87	0.915	XF-100	0.463
XF-113	0.307	XF-115	0.840
XF-118	0.321	XF-167	1.360
XF-169	0.620	ZST-1	0.708
ZST-2	0.637	ZST-4	0.296
ZST-5	0.770	ZST-6	1.090
ZST-7	1.350	ZST-8	0.867
ZST-9	1.035	ZST-10	0.798

[a] The spectroscopic binding values (K_d) were calculated by the Hanes−Woolf mapping method and repeated three times.

affinities of the drugs with CYP51, this may provide the basis for selective inhibition of compounds on different CYP51s. If the amino acid mutation occurred around the drug-binding site of the enzyme, it should decrease or increase the affinity of the drug, whereas a mutation affecting spatial structure would affect the binding of the enzyme with drug. Maybe the changes in the Tyr95, Phe206, and His293 amino acids are associated with resistance in the field for the triazoles.

The affinity of tebuconazole binding with the Y95F and F206L mutants was reduced, indicating the importance of these amino acids in the binding of UmCYP51 with tebuconazole. These results correspond with previously published results. The Tyr95 site was located on the B′ helix in SRS1 and might be related to its combination with substrate because *M. tuberculosis* Y76F/T/A/N could lead to the loss of enzyme activity (*25*). The site of Phe206 was on an F-helix, which contained many aromatic amino acids. Studies have shown that F-helices that contain a large number of aromatic amino acids may be the target of drugs for selective inhibition (*10*, *26*). Molecular modeling of *Candida albicans* CYP51 demonstrated that the F-helix F233/F235 was involved in binding with triazole drugs (*27*). For MtCYP51, a functional study of conserved amino acids in the F-helix showed that the mutations L172A/G/V and G175A/T reduced the activity of demethylation (*28*). Additionally, in mouse CYP51 a mutation at D231 in the F-helix led to changes in its activity (*29*). His293 was located in the SRS4 (−HTS−) (**Figure 5**) and was possibly the area responsible for substrate identification. The His293 site might be involved in maintaining the spatial structure of CYP51 given that the H293D mutant of UmCYP51 lacked the ability to bind with tebuconazole. A H314D/K/F/A mutation in mouse CYP51 led to decreased enzyme activity, presumably because this site might be necessary to maintain the correct conformation of CYP51 (*29*). The crystal structure of MtCYP51 analysis also showed that helix I was very important to the formation of the activity channel (*11*). The combination of site-directed mutagenesis with a binding assay provides a logical explanation for the affinity of different ligands for UmCYP51 and has allowed us to gain valuable insight into the interaction between fungicides and UmCYP51, which will be helpful in formulating strategies for designing specific drugs for UmCYP51 and understanding the mechanisms of resistance. Furthermore, the consistent results indicated that the template and all modeling strategies in the current study were reliable.

Screening of New DMI Fungicides Targeted UmCYP51. Absorption spectroscopy, which provided a simple and accurate method for determining the binding level of substrates and inhibitors to P450s, was examined at 25 °C. Addition of diniconazole and tebuconazole, azoles commonly used in agriculture for the treatment of pathogenic fungal infections of crops, to the samples containing UmCYP51 induced type II binding spectra with a maximum absorbance at 430 nm and a trough located at 400 nm (**Figure 5A**). Higher concentrations of tebuconazole and

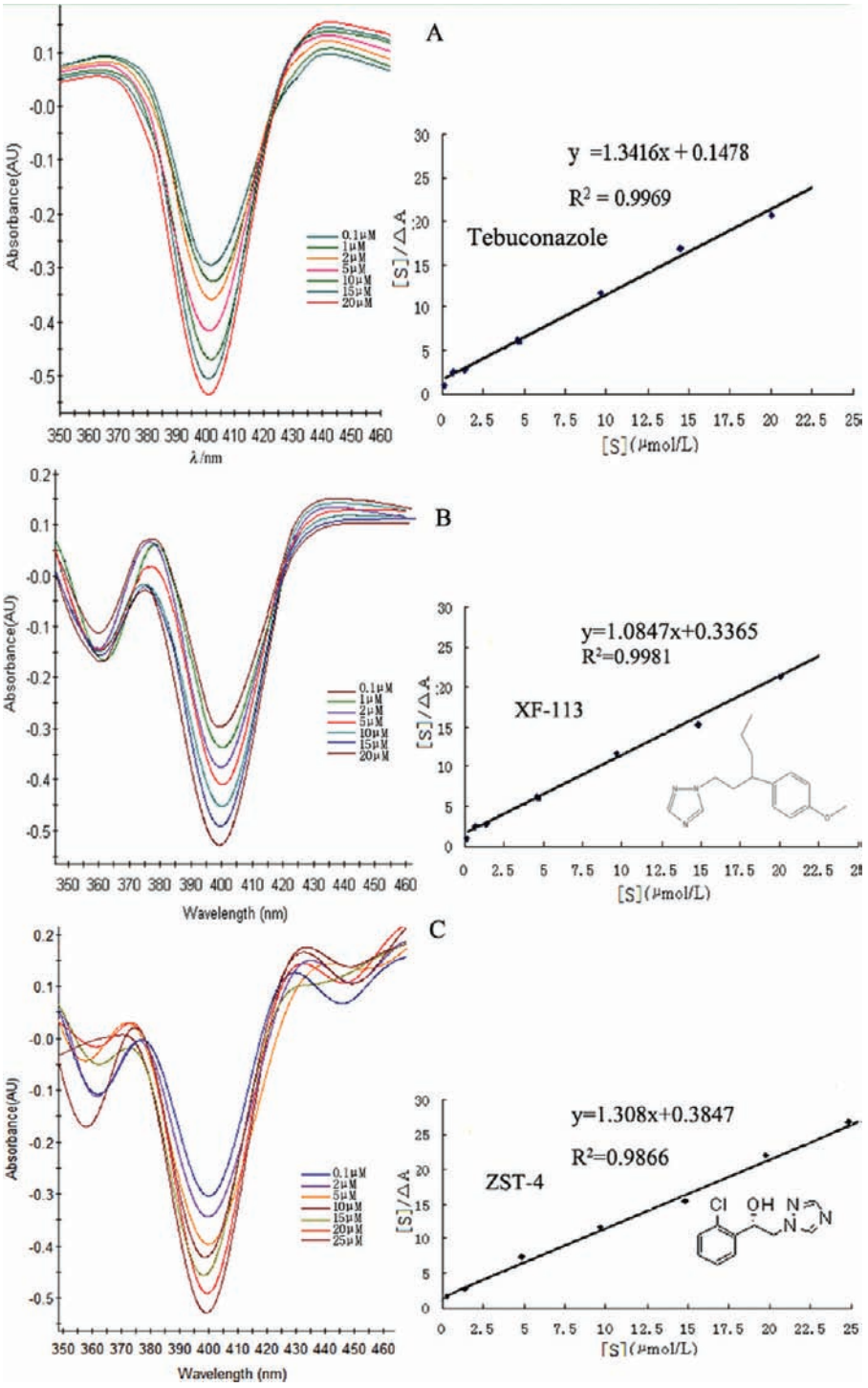

Figure 5. UmCYP51-35 type II binding spectrum in the presence of tebuconazole (**A**), XF-113 (**B**), and ZST-4 (**C**) respectively type II spectral response to tebuconazole, XF-113, and ZST-4 with the concentrations of 0.1, 1, 2, 5, 10, 15, and 20 μM from top to bottom. Hanes−Woolf plots were attained. ΔA = difference between the maximum absorbance and minimum absorbance. The binding studies were repeated three times, and the average changes in absorbance observed with each concentration of fungicides were calculated.

diniconazole resulted in a greater difference in absorbance values (Δ430−400), indicating a shift in the heme iron of the cytochrome P450 to a low-spin state on inhibitor binding. Red shift of the binding spectrum is probably due to the interaction between the triazole N4 of the fungicides and the heme of the P450. This exhibited the displacement of the native sixth ligand of the heme iron by the nitrogen atom in the triazole ring of tebuconazole (*3*, *7*). The spectral results showed that the affinity of tebuconazole and diniconazole with UmCYP51-35 was high, and the K_d values were calculated to be 0.110 and 0.255 μM, respectively (**Table 2**). Our data suggest that tebuconazole was the most sensitive fungicide for UmCYP51-35 among all of the tested compounds. Triadimenol and triadimefon binding to UmCYP51-35 resulted in a typical type I spectrum (data not shown).

We have reported that the XF and ZST series are two of the leading classes of antifungal compounds (*30*, *31*). Hence, the binding capacity of UmCYP51 with these compounds was tested. Our results demonstrated that XF-113 and ZST-4 had the best binding capacities to UmCYP51-35, with binding constants of 0.307 μM (**Figure 5B**) and 0.296 μM (**Figure 5C**), respectively.

These binding constants were close to those of the commercial fungicides, diniconazole and tebuconazole (**Table 2**), indicating that XF-113 and ZST-4 are candidates for the development of new fungicides.

Analysis of the binding abilities of synthetic XF and ZST fungicide lead compounds to *U. maydis* CYP51, the structure−activity relationships can be derived as follows: (I) In terms of ZST-4, the presence of groups such as chlorine at the ortho-position of a benzene ring can alter biological activity and lead to the tighter combination with UmCYP51 than others. (II) The absolute configuration of triazole compounds also shows an influence on the binding activity. For example, the *R*-enantiomer of XF-113 displayed tight binding with UmCYP51. These observations suggest that *U. maydis* CYP51 discriminates the enantiomers of XF-113 and that the *R*-enantiomer fits better in the active site of UmCYP51, which was consistent with PdCYP51 (*31*).

LITERATURE CITED

(1) Hargreaves, J. A.; Keon, J. P. R. Isolation of an *Ustilago maydis* ERG11 gene and its expression in a mutant decient in sterol 14α-demethylase activity. *FEMS Microbiol. Lett*. **1996**, *139*, 203−207.

(2) Galina, I. L.; Michael, R. W. CYP51—the omnipotent P450. *Mol. Cell. Endocrinol*. **2004**, *215*, 165−170.

(3) Ming, Z. H.; Xu, S. Z.; Zhou, L.; Ding, M. W.; Yang, J. Y.; Yang, S.; Xiao, W. J. Organocatalytic synthesis and sterol 14α-demethylase binding interactions of enantioriched 3-(1*H*-1,2,4-triazol-1-yl)butyl benzoates. *Bioorg. Med. Chem. Lett*. **2009**, *19*, 3938−3940.

(4) Zhu, J.; Lu, J. G.; Zhou, Y. J.; Li, Y. W.; Cheng, J.; Zheng, C. H. Design, synthesis, and antifungal activities in vitro of novel tetrahydroisoquinoline compounds based on the structure of lanosterol 14α-demethylase (CYP51) of fungi. *Bioorg. Med. Chem. Lett*. **2006**, *16*, 5285−5289.

(5) Lee, H.; Oh, H. J.; Ahn, H. M.; Oh, C. J.; Jeong, J. H.; Jeon, G. L.; An, C. S.; Choi, S. B.; Kim, H. B. A sterol biosynthetic gene AtCYP51A2 promoter for constitutive and ectopic expression of a transgene in plants. *J. Plant Biol*. **2008**, *51*, 359−365.

(6) Yang, J. Y.; Zhang, Q. Y.; Liao, M. J.; Xiao, M.; Xiao, W. J.; Yang, S.; Wan, J. Expression and homology modelling of sterol 14α-demethylase of *Magnaporthe grisea* and its interaction with azoles. *Pest Manag. Sci*. **2009**, *65*, 260−265.

(7) Zhao, L.; Liu, D. L.; Zhang, Q. Y.; Zhang, S.; Wan, J.; Xiao, W. J. Expression and homology modeling of sterol 14α-demethylase from *Penicillium digitatum*. *FEMS Microbiol. Lett*. **2007**, *277*, 37−43.

(8) Lee, C. H.; Hsu, K. H.; Wang, S. Y.; Chang, T. T.; Chu, F. H.; Shaw, J. F. Cloning and characterization of the lanosterol 14α-demethylase gene from *Antrodia cinnamomea*. *J. Agric. Food Chem*. **2010**, *58*, 4800−4807.

(9) Nistelrooy, J. G. M.; Brink, J. M.; Kan, J. A. L.; Gorcom, R. F. M.; Waard, M. A. Isolation and molecular characterisation of the gene encoding eburicol 14α-demethylase (CYP51) from *Penicillium italicum*. *Mol. Gen. Genet*. **1996**, *250*, 725−733.

(10) Lamb, D. C.; Kelly, D. E.; Manning, N. J.; Hollomon, D. W.; Kelly, S. L. Expression, purification, reconstitution and inhibition of *Ustilago maydis* sterol 14α-demethylase (CYP51; P450(14DM)). *FEMS Microbiol. Lett*. **1998**, *169*, 369−373.

(11) Ji, H. T.; Zhang, W. N; Zhou, Y. J.; Zhang, M.; Zhu, J.; Song, Y. L.; L, J. G. A three-dimensional model of lanosterol 14α-demethylase of *Candida albicans* and its interaction with azole antifungals. *J. Med. Chem*. **2000**, *43*, 2493−2505.

(12) Rupp, B.; Raub, S.; Marian, C.; Holtje, H.-D. Molecular design of two sterol 14α-demethylase homology models and their interactions with the azole antifungals ketoconazole and bifonazole. *J. Comput.-Aided Mol. Des*. **2005**, *19*, 149−163.

(13) Podust, L. M.; Poulos, T.; Waterman, M. R. Crystal structure of cytochrome P450 14α-sterol demethylase (CYP51) from *Mycobacterium tuberculosis* in complex with azole inhibitors. *Proc. Natl. Acad. Sci. U.S.A*. **2001**, *98*, 3068−3073.

(14) Strushkevich, N.; Usanov, S. A.; Park, H. W. Structural basis of human CYP51 inhibition by antifungal azoles. *J. Biol. Chem*. **2010**, *397*, 1067−1078.

(15) Lepesheva, G. I.; Park, H. W.; Hargrove, T. Y.; Vanhollebeke B.; Wawrzak, Z. Crystal structres of *Trypanosoma brucei* sterol 14α-demethylase and implication for selective treatment of human infections. *J. Biol. Chem*. **2009**, *285*, 1773−1780.

(16) Gasteiger, E.; Hoogland, C.; Gattiker, A.; Duvaud, S.; Wilkins, M. R.; Appel, R. D.; Bairoch, A. Protein identification and analysis tools on the ExPASy server. In *The Proteomics Protocols Handbook*; Walker, J. M., Ed.; Humana Press: Totowa, NJ, 2005; pp 571−607.

(17) Krogh, A.; Larsson, B.; Von, H. G.; Sonnhammer, E. L. Predicting transmembrane protein topology with a hidden Markov model: application to complete genomes. *J. Mol. Biol*. **2001**, *305*, 567−580.

(18) Huey, R.; Morris, G. M.; Olson, A. J.; Goodsell, D. S. A semiempirical free energy force field with charge-based desolvation. *J. Comput. Chem*. **2007**, *28*, 1145−1152.

(19) Braford, M. M.; McRorie, R. A.; Williams, W. L. A rapid and sensitive method for the quantification of microgram quantities of protein utilizing the principle of protein−dye binding. *Anal. Biochem*. **1976**, *72*, 248−254.

(20) Omura, T.; Sato, R. The carbon monoxide-binding pigment of liver microsomes. I. Evidence for its hemo protein nature. *J. Biol. Chem*. **1964**, *239*, 2370−2378.

(21) Korosec, T.; Acimovic, J.; Seliskar, M.; Kocjan, D.; Tacer, K. F.; Rozman, D.; Urleb, U. Novel cholesterol biosynthesis inhibitors targeting human lanosterol 14α-demethylase (CYP51). *Bioorg. Med. Chem. Lett*. **2008**, *16*, 209−221.

(22) Guardiola-Diaz, H. M.; Foster, L. A.; Mushrush, D.; Vaz, A. D. N. Azole-antifungal binding to a novel cytochrome P450 from *Mycobacterium tuberculosis*: implications for treatment of tuberculosis. *Biochem. Pharmacol*. **2001**, *61*, 1463−1470.

(23) Li, Y. C.; Chiang, J. Y. L. The expression of a catalytically active cholesterol 7α-hydroxylase cytochrome P450 in *Escherichia coli*. *J. Biol. Chem*. **1991**, *266*, 19186−19191.

(24) Venkateswarlu, K.; Lamb, D. C.; Kelly, D. E.; Manning, N. J.; Kelly, S. L. The N-terminal membrane domain of yeast NADPH-cytochrome P450 (CYP) oxidoreductase is not required for catalytic activity in sterol biosynthesis or in reconstitution of CYP activity. *J. Biol. Chem*. **1998**, *273*, 4492−4496.

(25) Lepesheva, G. I.; Virus, C.; Waterman, M. R. Conservation in the CYP51 family. Role of the B′ helix/BC loop and helices F and G in enzymatic function. *Biochemistry* **2003**, *42*, 9091−9101.

(26) Lamb, D. C.; Cannieux, M.; Warrilow, A. G. S.; Bak, S.; Kahn, R. A.; Manning, N. J.; Kelly, D. E.; Kelly, S. L. Plant sterol 14α-demethylase affinity for azole fungicides. *Biochem. Biophys. Res. Commun*. **2001**, *284*, 845−849.

(27) Lamb, D. C.; Kelly, D. E.; Baldwin, B. C. Differential inhibition of *Candida albicans* CYP51 with azole antifungal stereoisomers. *FEMS Microbiol Lett*. **1997**, *149*, 25−30.

(28) Bellamine, A.; Mangla, A. T.; Nes, W. D.; Waterman, M. R. Characterization and catalytic properties of the sterol 14α-demethylase from *Mycobacterium tuberculosis*. *Proc. Natl. Acad. Sci. U.S.A*. **1999**, *96*, 8937−8942.

(29) Nitahara, Y.; Kishimoto, K.; Yabusaki, Y.; Gotoh, O.; Yoshida, Y.; Horiuchi, T.; Aoyama, Y. The amino acid residues affecting the activity and azole susceptibility of rat CYP51 (sterol 14α-demethylase P450). *J. Biochem*. (*Tokyo*) **2001**, *129*, 761−768.

(30) Zhang, Q. Y.; Li, D.; Wei, P.; Zhang, J.; Wan, J.; Ren, Y. L.; Chen, Z. G.; Liu, D. L.; Yu, Z. N.; Feng, L. L. Structure-based rational screening of novel hit compounds with structural diversity for cytochrome P450 sterol 14α-demethylase from *Penicillium digitatum*. *J. Chem. Inf. Model*. **2010**, *50*, 317−325.

(31) Cao, X. F.; Hu, M.; Zhang, J.; Li, F.; Yang, Y. H.; Liu, D. L.; Liu, S. H. Determination of stereoselective interaction between enantiomers of chiral γ-aryl-1*H*-1,2,4-triazole derivatives and *Penicillium digitatum*. *J. Agric. Food Chem*. **2009**, *57*, 6914−6919.

Received for review August 20, 2010. Revised manuscript received November 10, 2010. Accepted November 10, 2010. This work was supported by grants from the Natural Science Foundation of China (30771429, 31071653), the National High Technology Research and Development Program of China (2007AA05Z417), the Key Technology Project in Hubei Province (2007AA201C50), and the Specialized Research Fund for the Doctoral Program of Higher Education (20060511002).